Shiraishi and Watanabe
Earth, Planets and Space (2023) 75:14
https://doi.org/10.1186/s40623-023-01772-0

Earth, Planets and Space

EXPRESS LETTER

Open Access

Seismic reflection imaging of deep crustal structures using local earthquakes in the Kanto region, Japan

Kazuya Shiraishi[1*] and Toshiki Watanabe[2]

Abstract

We applied a novel method of passive seismic reflection imaging to actual local earthquake data collected by a dense seismic network in the Kanto region, Japan. This method, which implements reverse time migration (RTM), is based on the cross-correlation of wavefields that are extrapolated forward and backward in time from receiver locations using passively observed seismic records. Using multiple reflections between the Earth's surface and subsurface boundaries, internal structures are imaged using many earthquakes without well-defined source information. The objective of this case study is to evaluate the possibility of acquiring seismic reflection images of the deep crustal structure by applying the RTM-based method using P-wave reflections in the earthquake data collected by a dense seismic network. The P-wave reflection profile along a 191-km-long pseudo-survey line down to a 100 km depth is obtained using the seismic records of hundreds of local earthquakes observed at 72 receiver stations. A P-wave velocity model for RTM imaging is extracted from an existing 3D model obtained by seismic tomography in a previous study. The resulting image shows several continuous reflectors at depths of 15–70 km. These reflectors correspond to the spatially variable velocity and suggest deep structures related to dual plate subduction in this region. Two eastward-dipping reflectors imaged at depths of 15–50 km are likely the top and bottom surfaces of the crust of the Philippine Sea slab, and the westward-dipping reflector at depths of 50–70 km implies the top surface of the Pacific slab. The en-échelon reflectors at depths of 15–20 km may be reflective boundaries between the upper and lower crust in the overlying Okhotsk plate. Our case study results confirm the possibility of obtaining profiles at higher resolutions than are typically obtained by earthquake-based seismic tomography and of imaging at depths beyond the limits of artificially controlled-source seismic surveys. Further implementation of the RTM-based imaging method will improve its potential use for subsurface imaging and monitoring from dense passive seismic data.

Keywords Seismic reflection imaging, Crustal structure, Local earthquake, Reverse time migration

*Correspondence:
Kazuya Shiraishi
kshiraishi@jamstec.go.jp
Full list of author information is available at the end of the article

Graphical Abstract

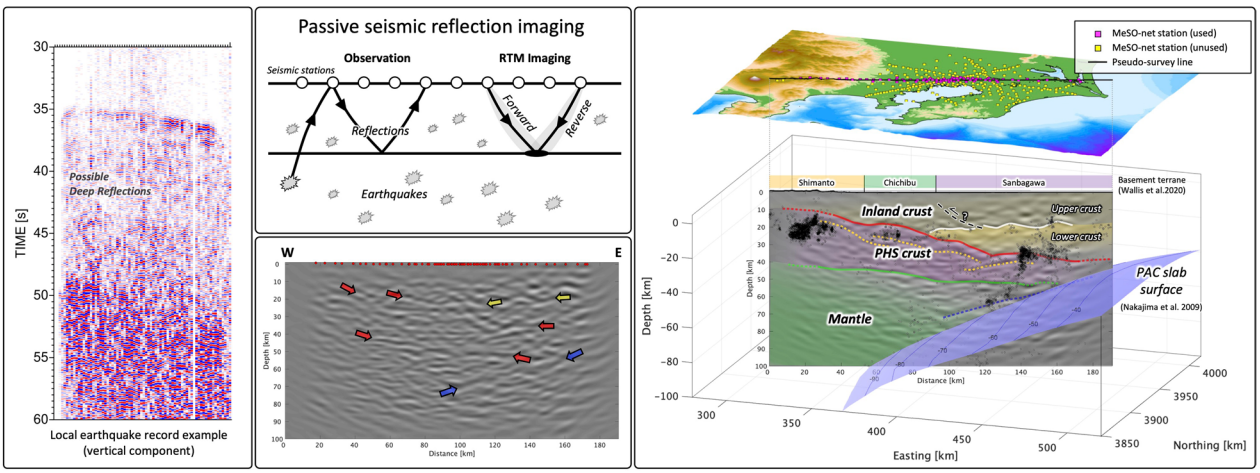

Introduction

Passively acquired seismic records, including those generated by earthquake events, have the potential to reveal deep crustal structures. Passive seismic tomography using earthquakes (e.g., Aki and Lee 1976; Dziewonski et al. 1977) is a major method for investigating the velocity structure of the Earth, and receiver function analysis (e.g., Langston 1979) is another popular method to image subsurface interfaces using multicomponent earthquake waveforms. While challenges remain in the use of reflection signals from seismic records for imaging deep subsurface structures, passive seismic reflection imaging is a promising technique for the acquisition of subsurface profiles with higher resolutions than other conventional earthquake-based methods. In addition, the large source energies released by earthquakes permit the imaging of structures that are deeper than those that can be imaged by artificial controlled sources, such as mechanical vibrators, airguns, or the explosives used in seismic surveys.

In dealing with passive seismic data, seismic interferometry (Wapenaar 2003; Campillo and Paul 2003; Schuster et al. 2004; Wapenaar and Fokkema 2006) is a useful method to reconstruct virtual source seismic survey data by correlating seismic records observed at different receivers. Then, subsequent processing techniques are applied for seismic reflection imaging. Successful applications of reflection imaging based on seismic interferometry using passive seismic data have been reported in previous studies using ambient seismic noise (e.g., Draganov et al. 2009, Poli et al. 2012), teleseismic data (Abe et al. 2007; Tonegawa et al. 2009; Ruigrok et al. 2010), and local earthquakes (Minato et al. 2012; Shiraishi et al. 2016; Maeda and Watanabe 2022). In the seismic interferometry approach, however, it is necessary to compute the cross-correlation of seismic records between all seismic stations before reflection imaging, which increases computational costs due to the number of receivers that act as virtual sources in both the data reconstruction and subsequent imaging process.

Direct imaging techniques using passive seismic data without prior cross-correlation in the data domain have been proposed that combine the concept of seismic interferometry with wavefield extrapolation in the image domain (Artman 2006; Burdick et al. 2014; Shiraishi 2015; Shiraishi and Watanabe 2022). Considering the fidelity of wavefield reconstruction by reverse time migration (RTM) (e.g., Chang and McMechan 1990), which is a powerful method for imaging complex subsurface structures in active-source seismic imaging (e.g., Etgen et al. 2009), Shiraishi and Watanabe (2022) developed an RTM-based direct imaging method for passive seismic records without earthquake source information. This method enables subsurface reflection imaging from earthquake records that contain multiple reflections between the Earth's surface and subsurface boundaries. They validated the acoustic and elastic RTM techniques in several realistic situations using numerical simulation.

The objective of this study is to evaluate the possibility of acquiring seismic reflection images of the deep crustal structure by applying the RTM-based method to actual local earthquake data collected from a dense seismic network. To this end, we apply the RTM-based imaging method to local earthquakes recorded by the dense Metropolitan Seismic Observation network (MeSO-net,

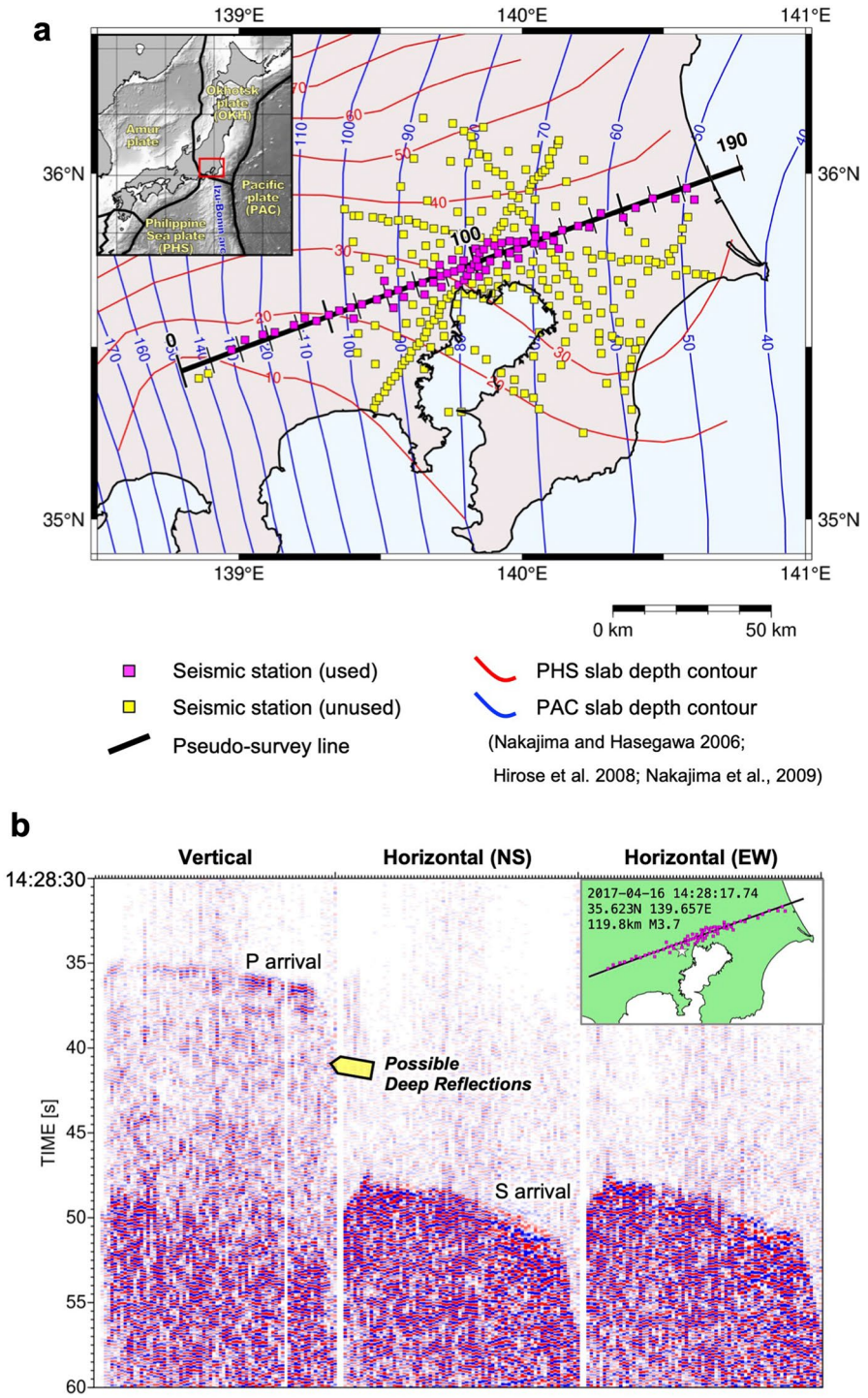

Fig. 1 Seismic observations from the Metropolitan Seismic Observation network (MeSO-net) in the Kanto region, Japan. **a** Seismic stations and depth contours of subducting slabs. The magenta and yellow squares denote the locations of MeSO-net stations (NIED 2021). Seventy-two stations (magenta squares) in a region 10 km wide along the pseudo-survey line (black bold line) are used for seismic imaging in this case study. The red and blue lines denote the depth contours of the Philippine Sea (PHS) slab and the Pacific (PAC) slab, respectively (Nakajima and Hasegawa 2006; Hirose et al. 2008; Nakajima et al. 2009). **b** Example of the earthquake records at the selected stations along the pseudo-survey line. Several coherent phases are observed after the P wave arrival, which should contain available reflections between the free-surface and subsurface boundaries

Fig. 1) with an average receiver spacing of 2–4 km (Sakai and Hirata 2009; Aoi et al. 2021) to image deep crustal structures in the Kanto region of Japan. The Philippine Sea (PHS) plate and the Pacific (PAC) plate are subducting beneath the Okhotsk (OKH) plate (Fig. 1), and many earthquakes related to dual plate subduction occur. Various subducting slab models have been developed by previous studies based on controlled-source seismic surveys (e.g., Sato et al. 2005; Kimura et al. 2010) and earthquake-based analyses, such as seismic tomography, receiver functions, and repeating earthquakes (e.g., Kimura et al. 2006; Nakajima and Hasegawa 2007; Hirose et al. 2008; Toda et al. 2008; Nakajima et al. 2009; Igarashi 2009; Uchida et al. 2010; Ito et al. 2019; Ishise et al. 2021). Our reflection imaging results add geophysical constraints to the crustal structure models that are deeper than those obtained from controlled-source surveys while also providing higher resolution profiles than those obtained by earthquake-based seismic tomography.

Methods

We apply an RTM-based method to local earthquake observations for passive seismic reflection imaging without source information (see Shiraishi and Watanabe 2022 for detailed descriptions with formulas). This technique allows imaging subsurface structures from passively observed earthquake records by receiver-side wavefield extrapolation using multiple reflections between the Earth's surface and subsurface boundaries. A reflection image at the subsurface point can be represented as a temporal integration of the product of two extrapolated wavefields at every time step. The forward wavefield and the backward wavefield are simulated with a velocity model using the observation record as the input waveform from each receiver location in the forward and reverse directions in time, respectively. Because superimposing the wavefields that are extrapolated from different receivers is possible for simultaneous observations with many receivers, only one computation is necessary for both receiver-side extrapolations from all receiver locations when using the same records. By stacking the integration results from many different earthquake records to illuminate the real reflectors and attenuate artifacts, we can obtain subsurface images directly from earthquake records without source information.

Considering P-wave reflection imaging based on acoustic assumptions, the receiver-side wavefields are computed by the finite difference method (FDM) (Mufti 1990) for the scalar wave equation using a P-wave velocity model. Shiraishi and Watanabe (2022) confirmed that the P-wave reflections are imaged at the correct depth for the subsurface boundaries even if the input data contain S-waves in the synthetic data tests, including P-to-S conversions, although they contain minor artifacts in the shallow portions due to source locations. The effects of S-waves and internal multiple reflections are minor, because their reflections are not effectively focused using P-wave velocities. They also suggested that using multi-component records with elastic RTM can eliminate artifacts due to S wave contamination. In current practical applications; however, it is still challenging to use elastic RTM with field data when dealing with actual three-component data. Here, we apply acoustic RTM using vertical component data for P-wave reflection imaging in the following case study.

Data

We use dense seismic data recorded by MeSO-net (Fig. 1) (National Research Institute for Earth Science and Disaster Resilience 2021). In this study, we set a 191-km-long pseudo-survey line in the SW–NE direction across a region of densely deployed stations and gathered seismic records from 72 stations that fell within a 10 km wide swath along that line (Fig. 1a). Due to the high density of the network, seismic records show that several coherent signals are clearly visible following the P-wave first arrival (Fig. 1b), especially on the vertical component. These signals should contain possible reflections between the free-surface and subsurface boundaries, thus enabling passive seismic reflection imaging.

We use 3 years of local earthquake records collected from April 2017 to March 2020 based on the Japan Meteorological Agency (JMA) unified earthquake catalog. First, we collect data for 722 earthquake events with 180 s long records and magnitudes over 2.5 in an approximately 180 km × 110 km area, including the MeSO-net stations (Fig. 2a, b). Then, we select 200 high-quality earthquake records from those 722 records according to the signal-to-noise ratio, as defined by the root-mean-square amplitude of the earthquake signals and background noises (Fig. 2c, d) once bad traces with abnormally high amplitude noise had been removed. After applying this selective filter, many of the 2.5–3.5

(See figure on next page.)

Fig. 2 Data selection of the local earthquakes. **a** Epicenter distribution and **b** source depth distribution of the local earthquakes. The gray dots are all events listed on the unified catalog of the Japan Meteorological Agency (JMA) from April 1, 2017, to March 31, 2020. The black dots are 772 earthquakes with magnitudes greater than 2.5, and the colored dots are the 200 high-quality events. **c** Four examples of vertical component records. The numbers in brackets correspond to the yellow dots with numbers in (**d**). **d** Signal-to-noise ratio (S/N) of the seismic records after being sorted in ascending order of S/N. Histograms of (**e**) magnitude and (**f**) depth distribution of all 722 events (gray bars) and the 200 high-quality events (red bars)

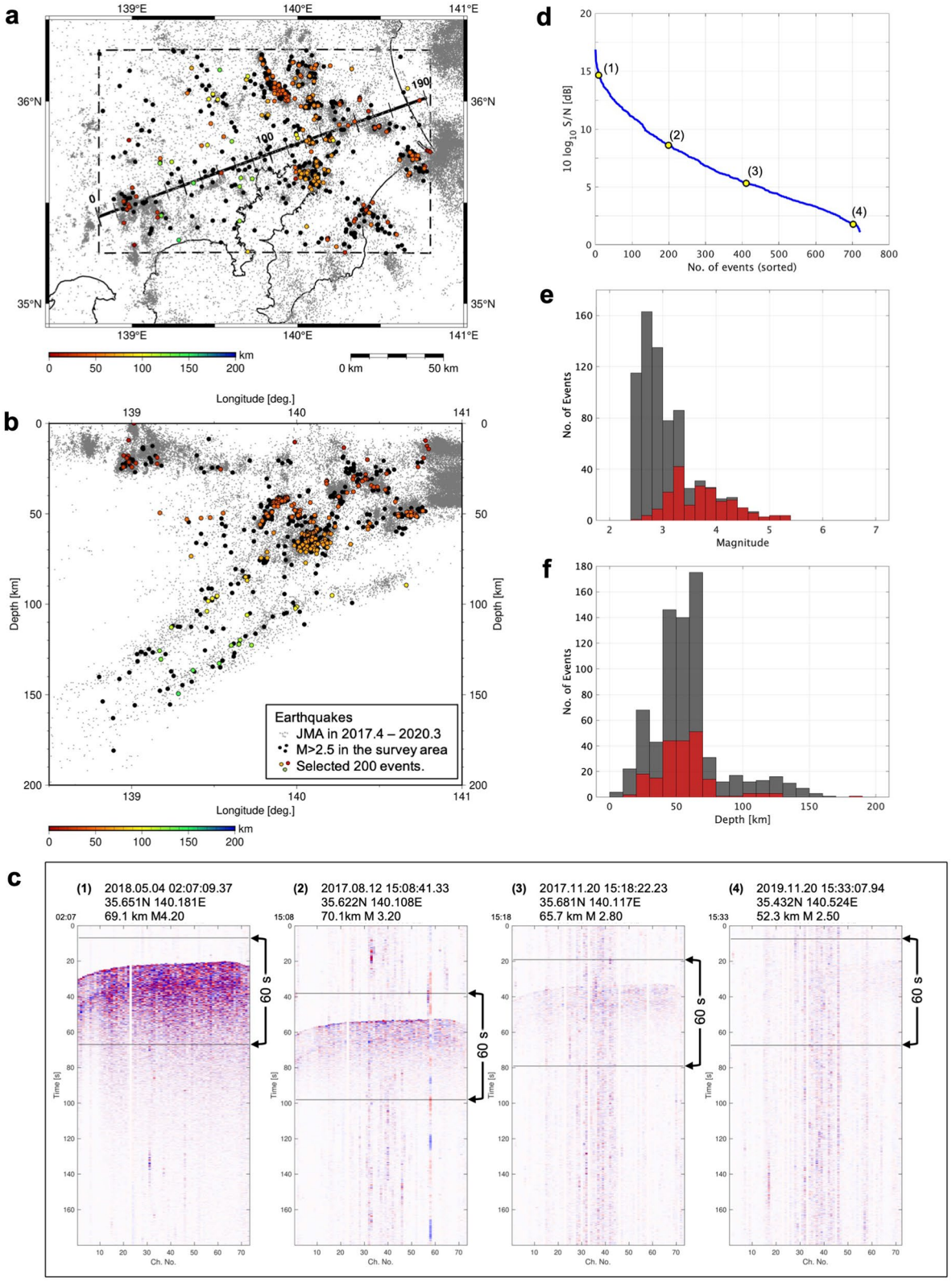

Fig. 2 (See legend on previous page.)

magnitude events are eliminated (Fig. 2e), and most of the selected earthquakes are shallower than 100 km (Fig. 2f). We use 60-s-long vertical component records that contain earthquake signals (Fig. 2c).

We note that spatial bias exists in the source distribution (Fig. 2a, b). Through our previous 2D numerical simulation with realistic situations, we recognized that the occurrence of artifacts due to sparse receivers was more severe than that due to source distribution (Shiraishi and Watanabe 2022). It is difficult to quantitatively clarify the effects from the biased source distribution, including the surrounding earthquakes in 3D. In this study, however, we expect better reflection illumination and artifact attenuation using as many local earthquakes as possible both beneath and surrounding the pseudo-survey line.

To model P-wave reflections by the two-dimensional acoustic RTM method, we prepare a P-wave velocity model extracted along the pseudo-survey line from an existing three-dimensional velocity model developed through earthquake-based seismic tomography (Matsubara et al. 2019). The extracted velocity model is interpolated from the original grid spacing of 0.1° in the horizontal direction and 2.5–15 km in the depth direction to 100 m × 100 m on the 191 km × 100 km vertical section. The 72 selected stations are then perpendicularly projected to the vertical section beneath the survey line. We consider that subsurface structures within a few km widths along the vertical section can be imaged by 2D RTM. To precondition the data, we apply a bandpass filter of 0.5–3 Hz and an automatic gain control with a 2-s gate to the 60-s vertical component records based on a previous investigation using 2D numerical simulations with realistic observation settings (Shiraishi and Watanabe 2022). Although the image resolution can be improved using higher frequencies, receiver-related artifacts appear due to spatial intervals between seismic stations. The preconditioned records were input simultaneously at all receiver locations to the forward and backward wavefield extrapolation for every earthquake event. To eliminate artifacts shown in the RTM image, such as low-frequency artifacts and steep-dip coherent artifacts, two-dimensional wavenumber domain filters were applied to the stacked section from all selected local earthquakes (Shiraishi and Watanabe 2022).

Results and discussion

Reflection profile from local earthquakes

Several continuous reflectors are visible at depths of 15–70 km on the final reflection profile (Fig. 3a); eastward-dipping reflectors at depths of 15–35 km and 40–50 km (red arrows), westward-dipping reflectors at depths of 50–70 km (blue arrows), and en-échelon reflectors at depths of 15–20 km in the eastern area (yellow arrows). The reflectors seem to correspond to the spatial variation of the velocity (Fig. 3b). The imaged reflectors imply impedance boundaries that are unclear in the smooth velocity model obtained by seismic tomography. To confirm that the tomography model is reasonable for reflection imaging and to check the imaging dependency on the velocities, we compared different velocity models with ± 10% scaling from the original velocity model for RTM imaging (Fig. 4). Velocity scaling from a base model is a common method to validate migration velocity models in seismic reflection imaging (e.g., Jones 2018). The velocity difference affects the focusing of reflections by seismic migration (i.e., amplitude and spatial continuity of reflection boundaries) in addition to the imaging depth of reflections (i.e., faster velocities increase the depth, and slower velocities decrease the depth). The reflectors imaged at depths of 15–50 km with the original velocity model (Fig. 4b) are obscure in other sections with the scaled velocity models (Fig. 4a, c). These reflectors that correspond to the spatial variation of velocity at depths of approximately 15–60 km should be reliable with less than 10% velocity errors compared to the original model. The westward-dipping reflector is visible at a depth of 50–80 km in the eastern part (Fig. 4c, light blue arrows), which may be deepened by increasing velocity compared to the original model (Fig. 4b, blue arrows). The eastward-dipping phases at depths of 50–80 km in the western part with decreased velocity (Fig. 4a, white arrows) could be reflectors or artifacts, and are not well-illuminated with the original velocity model (Fig. 4b). Although it is difficult to define accurate velocities from this velocity scaling test alone, the results suggest the possibility of refining the velocity in the deep portion in terms of reflection imaging. Indeed, non-negligible discrepancy in velocity values exists between several tomography models (e.g., Nakajima and Hasegawa 2007; Matsubara et al. 2019).

From the velocity scaling test, we conclude that the reflection profile using the velocity model by seismic tomography (Matsubara et al. 2019) is reasonable at depths from 15 km to 50–60 km. Further refinement of the migration velocity based on seismic tomography models will be helpful for improving reflection imaging of deep structures.

Structural interpretation in comparison with existing results

When comparing the reflection profile with the P-wave velocity (Matsubara et al. 2019) and the interpretation of the surfaces of the PHS and PAC slabs (Sato et al. 2005; Kimura et al. 2006; Igarashi et al. 2009, Nakajima et al. 2009), we see that some of the imaged reflectors are likely related to the PHS and PAC slabs (Fig. 5a, Additional file 1: Fig. S1). The upper eastward-dipping reflectors

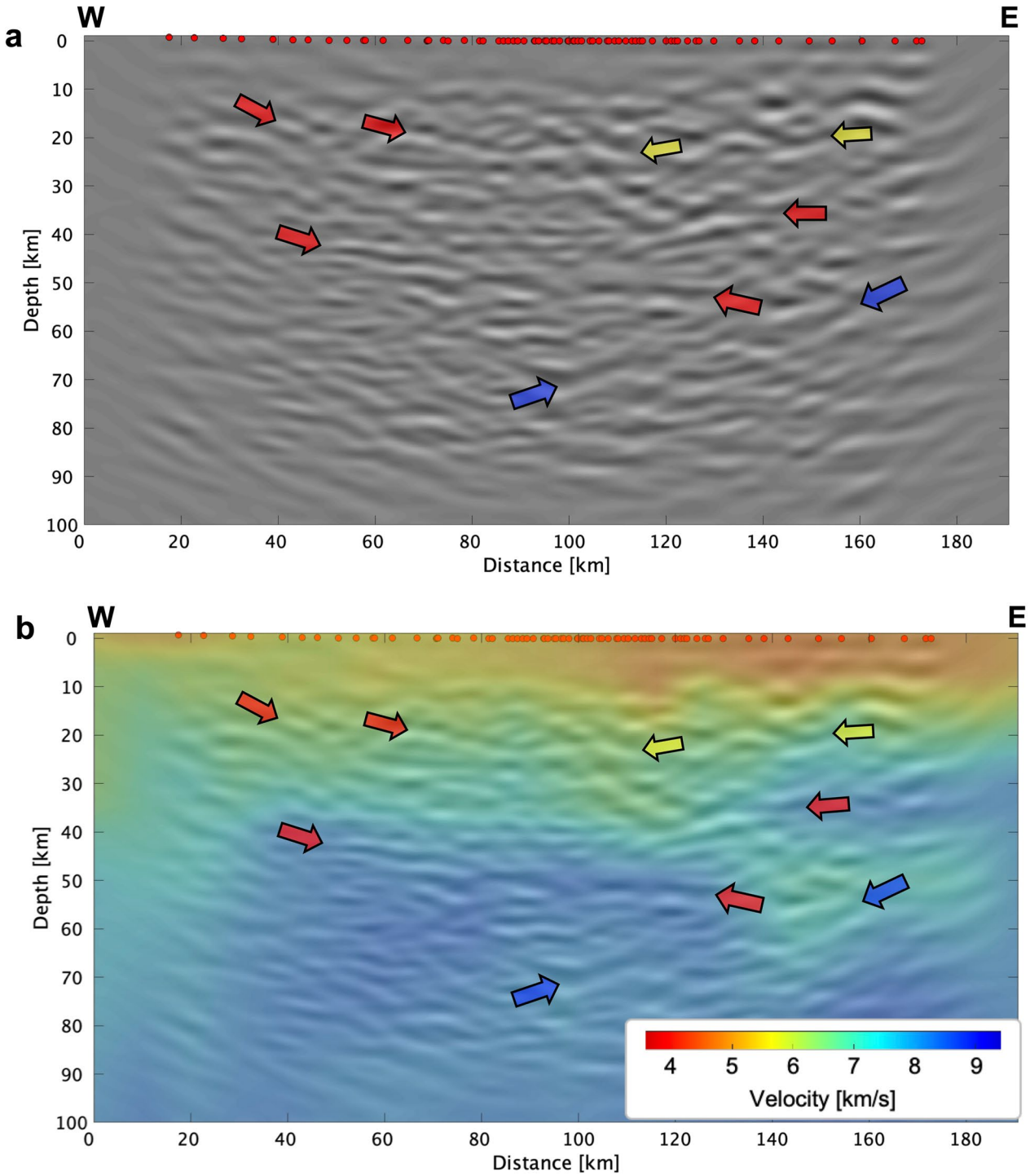

Fig. 3 Seismic reflection profile obtained by passive seismic reflection imaging with local earthquakes. **a** Final RTM section using 200 high-quality events and **b** final section overlaid with the P-wave velocity (Matsubara et al. 2019) used for RTM-based imaging. The red and blue arrows denote the eastward- and westward-dipping reflectors, respectively. The yellow arrows denote reflections with en-échelon pattern reflectors

(Fig. 5, red line) approximately correspond to the previous PHS surface models inferred from the controlled-source reflection survey (Sato et al. 2005) and analysis of repeating earthquakes and receiver functions (Kimura et al. 2006; Igarashi 2009) (Fig. 5a). They also seem to correspond to the top of the lower-velocity zone compared

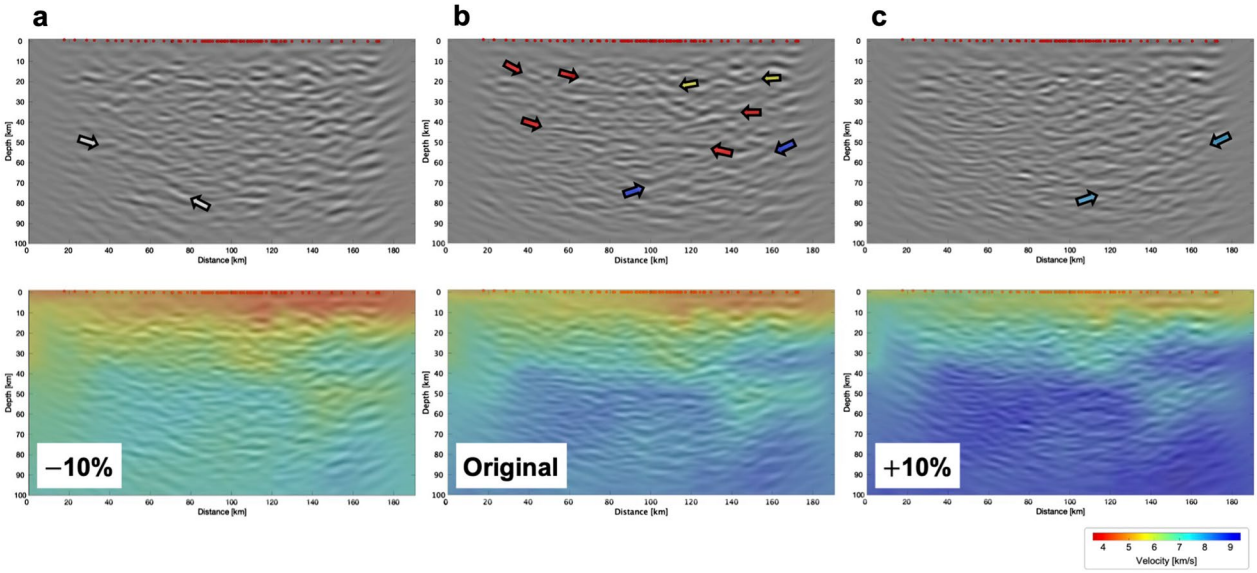

Fig. 4 Comparison of the RTM images with different velocity models. The RTM results with the velocity models of (**a**) − 10% scaling, (**b**) original, and (**c**) + 10% scaling. The upper panels show RTM sections, and the lower panels show the same sections overlaid with the scaled velocity models. The red, blue and yellow arrows in (**b**) denote the eastward- and westward-dipping reflectors and en-échelon pattern reflectors, respectively, which are visible using the original velocity model. The light blue arrows in (**c**) indicate the west-dipping reflector that corresponds to that indicated by the blue arrows in (**b**) and is imaged deeper by higher velocity. The white arrows in (**a**) denote the eastward-dipping phases that do not clearly correspond to the reflection profile with the original velocity

to the one-dimensional velocity model at depths of 20–30 km in the middle part of the velocity perturbation model (Additional file 1: Figures S1, S2). The upper reflector (red line) is located a few km shallower than the previously suggested PHS surface (Fig. 5, magenta line) in the western to middle part, and they converge on the eastern side, where most of the interpretations are similar around a 35 km depth. The possibility of a shallower depth of the PHS surface than that of Nakajima et al. (2009) was also suggested by Ishise et al. (2021) based on their anisotropic seismic tomography model. The depth of the upper reflector is approximately consistent with those of the PHS surface around the intersecting points in previous studies that use complementary techniques and data sets (Sato et al. 2005; Ishise et al. 2021; Kimura et al. 2006) (Fig. 5b). Consequently, the upper eastward-dipping reflector (red line) is likely the top of the PHS slab.

The lower eastward-dipping reflector at depths of 40–50 km (Fig. 5, green line), which seems to correspond to inflection points of the vertical velocity profiles (Additional file 1: Figure S2), may indicate the bottom of the crust of the PHS slab, although different interpretations exist (e.g., Toda et al. 2008; Nakajima et al. 2009; Ishise et al. 2021). The thickness of the inferred PHS crust from 30 km in the west to 20 km in the east (Fig. 5b) may correspond to the northern part of the Izu-Bonin arc in the eaten side of the PHS plate (top-left panel in Fig. 1a) with a thickness of ~ 20 km to ~ 35 km that was revealed by marine wide-angle seismic surveys across and along the Izu-Bonin arc (Suyehiro et al. 1996; Kodaira et al. 2007; Tamura et al. 2016). The reflectors subparallel to the top of the PHS crust might be unit boundaries within the PHS crust due to the crustal structures in the northward extension of the Izu-Bonin arc (Fig. 5, orange dashed lines).

Although ambiguity exists in the imaged depth as mentioned above, the westward-dipping reflector at depths of 50–70 km (Fig. 5a, blue dashed line) can be interpreted as the surface of the PAC slab at approximately the same depth as in the previous models that were based on seismic tomography (Nakajima et al. 2009) (Fig. 5a, black dashed line) and on receiver functions and repeating earthquake data (Igarashi 2009) (Fig. 5a, blue squares).

The en-échelon reflectors at depths of 15–20 km in the eastern part above the PHS slab (Fig. 5, white lines) imply a reflective zone around the boundary between the upper and lower crusts, which can be identified in the controlled-source seismic survey results (Sato et al. 2005; Kimura et al. 2010). The en-échelon pattern of the reflectors might represent the lower boundary of the basement terranes beneath Kanto (Wallis et al. 2020).

Some of the imaged reflection boundaries correspond well to previous studies, and they suggest the existence of

impedance contrasts that are not imaged in the regional smooth velocity models derived by seismic tomography. Our imaging results imply possible reflection boundaries that are deeper than those from controlled-source surveys while also providing higher resolution profiles than those obtained by earthquake-based analyses, such as seismic tomography and receiver functions. The depths of interpreted boundaries are not always consistent with other imaging results and interpretations. Imaging depth and resolution are highly dependent on the sources, grid size, velocity, and other parameters for each method. A complementary investigation using different approaches with controlled-source and passive-source seismic data is important for better understanding deep structures.

Further application possibilities

The results of our case study confirm the possibility of obtaining reflection profiles of deep crustal structures from local earthquakes. When collecting earthquake records for passive source imaging, one should consider that local earthquake records are often widely available and have good quality and wider frequency components than teleseismic earthquakes. However, the effects of S-waves within local earthquake data are not negligible, even though P-waves are dominantly focused by acoustic RTM using a P-wave velocity model (Shiraishi and Watanabe 2022). To eliminate artifacts due to S waves in P-wave reflection imaging, the selective use of very deep local earthquakes or teleseismic events will be useful due to the longer source-related lag time between the P-wave and S-wave arrivals than that of local earthquakes (Maeda and Watanabe 2022). On the other hand, the S-wave coda can be used to improve the spatial resolution of reflection profiles. Elastic RTM should be applied to multi-component passive seismic data to address both P- and S-waves (Shiraishi and Watanabe 2022) and eventually used for 3D models. We note that spatial bias exists in the source distribution due to the use of earthquakes and uneven spatial sampling in actual seismic observations in 3D (e.g., Figs. 1, 2a, b). The effects of a biased source distribution and uneven spatial sampling in complex geological structures should also be studied through 3D numerical simulation. Furthermore, the possibility of subsurface reflection imaging with continuous passive seismic records suggests the potential for time-lapse surveys or continuous monitoring of subsurface structures and physical properties (Shiraishi 2015; Tonegawa et al. 2021). Regular monitoring and profiling by quasi-real-time RTM-based processing could be implemented by combining data preconditioning with automatic event detection from continuous records from a seismic network (e.g., Mousavi et al. 2020) to assist in certain aspects of environmental and disaster mitigation. These implementations will improve the applicability of the proposed method in investigating subsurface structures and conditions with dense seismic observations.

Conclusion

We applied the RTM-based reflection imaging method to actual local earthquake records observed by the dense seismic station network in the metropolitan area of Japan. We successfully obtained a reflection profile that showed continuous reflectors that corresponded to the spatial variation in the velocity model derived in previous studies. The reflection profile suggested some new insights into the investigation of deep crustal structures involving dual plate subduction. The eastward- and westward-dipping reflectors imaged at depths of 15–70 km likely correspond to the PHS and PAC slabs, respectively. The thickness of 20–30 km between the possible upper and bottom surfaces of the crust of the PHS slab implies the northern extension of the thick crust of the Izu-Bonin arc. The en-échelon reflectors in the shallower part of the 15–20 km depth interval may suggest reflective zones at the boundary between the upper and lower crust beneath the Kanto Basin. The results confirmed the possibility of obtaining profiles at higher resolutions than could be obtained by seismic tomography and imaging depths

(See figure on next page.)

Fig. 5 Structural interpretation of the reflection profile. **a** Final RTM section overlaid with the P-wave velocity (Matsubara et al. 2019). **b** Three-dimensional view of the interpreted reflection profile with the topography map in the Kanto region. The red and green lines corresponding to the eastward-dipping reflectors are interpreted as the top and bottom surfaces of the PHS crust, respectively. The depth of the PHS top surface is approximately consistent with that at intersecting points in previous studies (Sato et al. 2005; Kimura et al. 2006; Ishise et al. 2021). The orange dotted lines subparallel to the upper eastward-dipping reflector may be some unit boundaries within the PHS crust due to the crustal structures in the northward extension of the Izu-Bonin arc. The blue dotted line for the westward-dipping reflector is interpreted as the top of the PAC slab. The white lines indicate the en-échelon reflectors interpreted as the boundary between the upper and lower crust in the inland crust beneath the Kanto region. The yellow dot in (**a**) shows the depth of the PHS surface inferred by the seismic reflection survey (Sato et al. 2005). The green dot in (**a**) indicates the depth of the PHS slab surface inferred from repeated earthquakes (Kimura et al. 2006). The red and blue rectangles in (**a**) denote the depths of the PHS and PAC slab surfaces, respectively, which are read from the interpretation of receiver function analysis and repeating earthquakes (Igarashi et al. 2009). The magenta and black dashed lines indicate the PHS and PAC slab surfaces, respectively, in (**a**), and the translucent blue surface with contours shows the PAC slab surface in (**b**) of the previous interpretation of earthquake-based seismic tomography (Nakajima and Hasegawa 2006; Hirose et al. 2008; Nakajima et al. 2009). The black dots in (**b**) denote the sources projected to the RTM section from all earthquakes from the JMA catalog in the range of 10 km wide along the pseudo-survey line

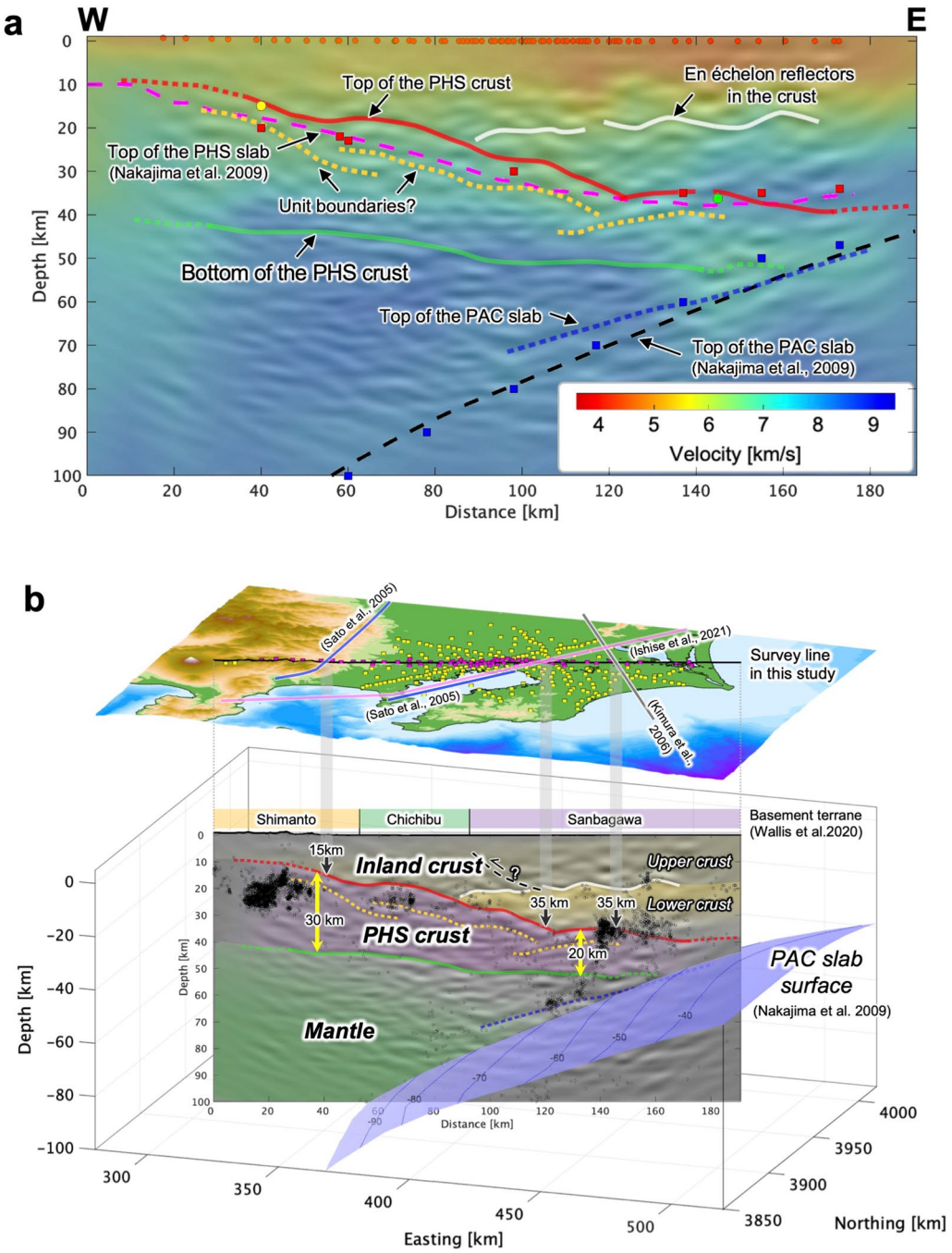

Fig. 5 (See legend on previous page.)

beyond the limits of controlled-source seismic surveys. To better investigate detailed geological structure features, further implementations may improve image quality by refining the migration velocities and eventually dealing with elastic waves in three dimensions.

Abbreviations

FDM	Finite difference method
JMA	Japan Meteorological Agency
MeSO-net	Metropolitan Seismic Observation network
NIED	National Research Institute for Earth Science and Disaster Resilience
PAC	Pacific
PHS	Philippine Sea

RMS	Root mean square
RTM	Reverse time migration
2D	Two-dimensions or two-dimensional
3D	Three-dimensions or three-dimensional

Supplementary Information

The online version contains supplementary material available at https://doi.org/10.1186/s40623-023-01772-0.

Additional file 1. Supplementary figures S1 and S2

Acknowledgements

This research is supported by the Japan Society for the Promotion of Science (JSPS) KAKENHI Grant-in-Aid for Scientific Research (c) (JP19K04028). We used information on the earthquake source location from the Japan Meteorological Agency (JMA) unified catalog and seismic records of the Metropolitan Seismic Observation network (MeSO-net) managed by the National Research Institute for Earth Science and Disaster Resilience (NIED). We are grateful for constructive comments from Pascal Audet and two anonymous reviewers that have improved the manuscript.

Author contributions

KS processed the data and drafted the manuscript in discussions with TW. Both authors read and approved the final manuscript.

Funding

Japan Society for the Promotion of Science (JSPS) Grant-in-Aid for Scientific Research (c), Grant Number JP19K04028.

Availability of data and materials

Seismic waveform data of MeSO-net used in this study are available from the NIED website (https://doi.org/10.17598/NIED.0023). Processed results are available by request to the corresponding author.

Declarations

Ethics approval and consent to participate

Not applicable.

Consent for publication

Not applicable.

Competing interests

The authors declare that they have no competing interests.

Author details

[1]Japan Agency for Marine-Earth Science and Technology (JAMSTEC), Research Institute for Marine Geodynamics, 3173-25, Showa-Machi, Kanazawa-Ku, Yokohama-City, Kanagawa 236-0001, Japan. [2]Earthquakes and Volcano Research Center, Graduate School of Environmental Studies, Nagoya University, Furo-cho, Chikusa-ku, Nagoya, Aichi 464-8601, Japan.

Received: 22 September 2022 Accepted: 14 January 2023
Published online: 28 January 2023

References

Abe S, Kurashimo E, Sato H, Hirata N, Iwasaki T, Kawanaka T (2007) Interferometric seismic imaging of crustal structure using scattered teleseismic waves. Geophys Res Lett 34:L19305. https://doi.org/10.1029/2007GL030633

Aki K, Lee W (1976) Determination of three-dimensional velocity anomalies under a seismic array using first P arrival times from local earthquakes, 1. A homogeneous initial model. J Geophys Res 81:4381–4399. https://doi.org/10.1029/JB081i023p04381

Aoi S, Kimura T, Ueno T, Senna S, Azuma H (2021) Multi-data integration system to capture detailed strong ground motion in the Tokyo metropolitan area. J Disaster Res 16:684–699. https://doi.org/10.20965/jdr.2021.p0684

Artman B (2006) Imaging passive seismic data. Geophysics 71:SI177–SI187. https://doi.org/10.1190/1.2209748

Burdick S, de Hoop MV, Wang S, van der Hilst RD (2014) Reverse-time migration-based reflection tomography using teleseismic free surface multiples. Geophys J Int 196:996–1017. https://doi.org/10.1093/gji/ggt428

Campillo M, Paul A (2003) Long-range correlations in the diffuse seismic coda. Science 299:547–549. https://doi.org/10.1126/science.1078551

Chang WF, McMechan G (1990) 3D acoustic prestack reverse-time migration. Geophys Prosp 38:737–755. https://doi.org/10.1111/j.1365-2478.1990.tb01872.x

Draganov D, Campman X, Thorbecke J, Verdel A, Wapenaar K (2009) Reflection images from ambient seismic noise. Geophysics 74(5):A63–A67. https://doi.org/10.1190/1.3193529

Dziewonski A, Hager B, O'Connell R (1977) Large-scale heterogeneities in the lower mantle. J Geophys Res 82:239–255. https://doi.org/10.1029/JB082i002p00239

Etgen J, Gray SH, Zhang Y (2009) An overview of depth imaging in exploration geophysics. Geophysics 74:WCA5–WCA17. https://doi.org/10.1190/1.3223188

Hirose F, Nakajima J, Hasegawa A (2008) Three-dimensional velocity structure and configuration of the Philippine sea slab beneath Kanto District, Central Japan, estimated by double-difference tomography (in Japanese with English abstract). Zisin 60:123–138. https://doi.org/10.4294/zisin.60.123

Igarashi T (2009) Seismic velocity discontinuities in the crust and uppermost mantle beneath the Kanto district, central Japan, identified from receiver function imaging and repeating earthquake activity. Gondwana Res 16:491–503. https://doi.org/10.1016/j.gr.2009.03.005

Ishise M, Kato A, Sakai S, Nakagawa S, Hirata N (2021) Improved 3-D P wave azimuthal anisotropy structure beneath the Tokyo metropolitan area, Japan: new interpretations of the dual subduction system revealed by seismic anisotropy. J Geophys Res Solid Earth. https://doi.org/10.1029/2020JB021194

Ito A, Tonegawa T, Uchida N, Yamamoto Y, Suetsugu D, Hino R, Sugioka H, Obana K, Nakahigashi K, Shinohara M (2019) Configuration and structure of the Philippine Sea Plate off Boso, Japan: constraints on the shallow subduction kinematics, seismicity, and slow slip events. Earth Planets Space 71:111. https://doi.org/10.1186/s40623-019-1090-y

Jones IF (2018) Velocities, imaging, and waveform inversion: the evolution of characterizing the Earth's subsurface. App 1. EAGE publications, Houten, Netherlands. https://doi.org/10.3997/book9789462822535

Kimura H, Kasahara K, Igarashi T, Hirata N (2006) Repeating earthquake activities associated with the Philippine Sea plate subduction in the Kanto district, central Japan: a new plate configuration revealed by interplate aseismic slips. Tectonophysics 417:101–118. https://doi.org/10.1016/j.tecto.2005.06.013

Kimura H, Takeda T, Obara K, Kasahara K (2010) Seismic evidence for active underplating below the megathrust earthquake zone in Japan. Science 329(5988):210–212. https://doi.org/10.1126/science.1187115

Kodaira S, Sato T, Takahashi N, Ito A, Tamura Y, Tatsumi Y, Kaneda Y (2007) Seismological evidence for variable growth of crust along the Izu intraoceanic arc. J Geophys Res 112:B05104. https://doi.org/10.1029/2006JB004593

Langston CA (1979) Structure under Mount Rainier, Washington, inferred from teleseismic body waves. J Geophys Res 84:4749–4762. https://doi.org/10.1029/JB084iB09p04749

Maeda Y, Watanabe T (2022) Estimating errors in autocorrelation functions for reliable investigations of reflection profiles. Earth Planets Space 74:48. https://doi.org/10.1186/s40623-022-01606-5

Matsubara M, Sato H, Uehira K, Mochizuki M, Kanazawa T, Takahashi N, Suzuki K, Kamiya S (2019) Seismic velocity structure in and around the Japanese Island arc derived from seismic tomography including NIED MOWLAS Hi-net and S-net data. Seismic Waves—Probing Earth System. IntechOpen. https://doi.org/10.5772/intechopen.86936

Minato S, Tsuji T, Matsuoka T, Obana K (2012) Crosscorrelation of earthquake data using stationary phase evaluation: Insight into reflection structures

of oceanic crust surface in the Nankai Trough. Int J Geophy 2012:101545. https://doi.org/10.1155/2012/101545
Mousavi SM, Ellsworth WL, Zhu W, Chuang LY, Beroza GC (2020) Earthquake transformer—an attentive deep-learning model for simultaneous earthquake detection and phase picking. Nature Comm 11:3952. https://doi.org/10.1038/s41467-020-17591-w
Mufti IR (1990) Large-scale three-dimensional seismic models and their interpretive significance. Geophysics 55:1166–1182. https://doi.org/10.1190/1.1442933
Nakajima J, Hasegawa A (2006) Anomalous low-velocity zone and linear alignment of seismicity along it in the subducted Pacific slab beneath Kanto, Japan: reactivation of subducted fracture zone? Geophys Res Lett 33:L16309. https://doi.org/10.1029/2006GL026773
Nakajima J, Hasegawa A (2007) Subduction of the Philippine Sea plate beneath southwestern Japan: slab geometry and its relationship to arc magmatism. J Geophys Res 112:B08306. https://doi.org/10.1029/2006JB004770
Nakajima J, Hirose F, Hasegawa A (2009) Seismotectonics beneath the Tokyo metropolitan area, Japan: effect of slab-slab contact and overlap on seismicity. J Geophys Res 114:B08309. https://doi.org/10.1029/2008JB006101
National Research Institute for Earth Science and Disaster Resilience (2021) NIED MeSO-net, National Research Institute for Earth Science and Disaster Resilience. https://doi.org/10.17598/NIED.0023
Poli P, Campillo M, Pedersen H, LAPNET Working Group (2012) Body-wave imaging of Earth's mantle discontinuities from ambient seismic noise. Science 338:1063–1065. https://doi.org/10.1126/science.1228194
Ruigrok E, Campman X, Draganov D, Wapenaar K (2010) High-resolution lithospheric imaging with seismic interferometry. Geophys J Int 183:339–357. https://doi.org/10.1111/j.1365-246X.2010.04724.x
Sakai S, Hirata N (2009) Distribution of the metropolitan seismic observation network (in Japanese with English abstract). Bull Earthq Res Inst 84:57–69. https://doi.org/10.15083/0000032433
Sato H, Hirata N, Koketsu K, Okaya D, Abe S, Kobayashi R, Matsubara M, Iwasaki T, Ito T, Ikawa T, Kawanaka T, Kasahara K, Harder S (2005) Earthquake source fault beneath Tokyo. Science 309:462–464. https://doi.org/10.1126/science.1110489
Schuster GT, Yu J, Sheng J, Rickett J (2004) Interferometric/daylight seismic imaging. Geophys J Int 157:838–852. https://doi.org/10.1111/j.1365-246X.2004.02251.x
Shiraishi K, Watanabe T (2022) Passive seismic reflection imaging based on acoustic and elastic reverse time migration without source information: theory and numerical simulations. Explor Geophys 53:198–210. https://doi.org/10.1080/08123985.2021.1917293
Shiraishi K, Abe S, Takahashi T, Tsumura N, Ito T (2016) Subsurface exploration with P-coda of local earthquakes using seismic interferometry (in Japanese with English abstract). BUTSURI-TANSA 69:249–268. https://doi.org/10.3124/segj.69.249
Shiraishi K (2015) Seismic interferometry in image domain based on reverse time migration for passive seismic monitoring. 77th EAGE Ext abs Th N108 11. https://doi.org/10.3997/2214-4609.201413260
Suyehiro K, Takahashi N, Ariie Y, Yokoi Y, Hino R, Shinohara M, Kanazawa T, Hirata N, Tokuyama H, Taira A (1996) Continental crust, crustal underplating, and low-Q upper mantle beneath an oceanic island arc. Science 272:390–392. https://doi.org/10.1126/science.272.5260.390
Tamura Y, Sato T, Fujiwara T, Kodaira S, Nichols A (2016) Advent of continents: a new hypothesis. Sci Rep 6:33517. https://doi.org/10.1038/srep33517
Toda S, Stein R, Kirby S, Bozkurt SB (2008) A slab fragment wedged under Tokyo and its tectonic and seismic implications. Nature Geosci 1:771–776. https://doi.org/10.1038/ngeo318
Tonegawa T, Nishida K, Watanabe T, Shiomi K (2009) Seismic interferometry of teleseismic S-wave coda for retrieval of body waves: an application to the Philippine Sea slab underneath the Japanese Islands. Geophys J Int 178:1574–1586. https://doi.org/10.1111/j.1365-246X.2009.04249.x
Tonegawa T, Kimura T, Shiraishi K, Yabe S, Fukao Y, Araki E, Kinoshita M, Sanada Y, Miura S, Nakamura Y, Kodaira S (2021) Weak faults at megathrust plate boundary respond to tidal stress. Earth Planets Space 73:89. https://doi.org/10.1186/s40623-021-01414-3
Uchida N, Matsuzawa T, Nakajima J, Hasegawa A (2010) Subduction of a wedge-shaped Philippine Sea plate beneath Kanto, central Japan, estimated from converted waves and small repeating earthquakes. J Geophys Res 115:B07309. https://doi.org/10.1029/2009JB006962
Wallis SR, Yamaoka K, Mori H, Ishiwatari A, Miyazaki K, Ueda H (2020) The basement geology of Japan from A to Z. Island Arc. 29:e12339. https://doi.org/10.1111/iar.12339
Wapenaar K (2003) Synthesis of an inhomogeneous medium from its acoustic transmission response. Geophysics 68:1756–1759. https://doi.org/10.1190/1.1620649
Wapenaar K, Fokkema J (2006) Green's function representations for seismic interferometry. Geophysics 71:SI33–SI46. https://doi.org/10.1190/1.2213955

Publisher's Note